Chemical Science

ROYAL SOCIETY OF CHEMISTRY

EDGE ARTICLE

View Article Online
View Journal | View Issue

Cite this: *Chem. Sci.*, 2025, **16**, 3705

All publication charges for this article have been paid for by the Royal Society of Chemistry

Received 16th December 2024
Accepted 19th January 2025

DOI: 10.1039/d4sc08496a

rsc.li/chemical-science

Palladium-catalyzed intramolecular aerobic oxidative cross-coupling of BH/CH between *o*-carborane and arenes†

Zhen Wang,[ab] Jiahui Yu,[c] Jie Zhang,[d] Dengsong Zhang,[c] Zaozao Qiu *[bc] and Zuowei Xie *[be]

An efficient Pd-catalyzed regioselective intramolecular aerobic oxidative dehydrocoupling of BH/CH between *o*-carborane and arenes has been achieved with the construction of a series of five-, six- and seven-membered rings under mild reaction conditions. Control experiments indicate that B–H activation proceeds preferentially over the aryl C–H. These new polyarene–carborane conjugates have potential applications in materials as demonstrated by pyrene fused *o*-carborane that exhibits unique dual-phase emission, intramolecular charge transfer (ICT), and aggregation-induced emission (AIE) properties.

Introduction

Carboranes are a class of polyhedral boron hydride molecular clusters in which one or more of the BH vertices are replaced by CH units.[1] Their structural features, such as spherical geometry and three-dimensional electron delocalization, make them valuable components in various applications, ranging from functional materials to pharmaceuticals.[2,3] The *o*-carborane unit is known for its distinct electronic characteristics, including steric electronic conjugation and position-dependent electron-donating and accepting properties.[4] Due to the electronic interactions between the carborane unit and the attached π-conjugated substituents, *o*-carboranes have gained significant interest as a versatile boron element-block for constructing optoelectronic materials, especially for their remarkable ability to suppress aggregation-caused quenching (ACQ). This feature is mainly observed in carbon vertex-substituted derivatives.[5] However, the limited functionalization methods for boron vertex-arylated *o*-carboranes restrict their further applications.[6]

Among the various methodologies developed for *o*-carborane B–H activation, transition-metal-catalyzed BH/CH oxidative coupling is regarded as the most direct and efficient method for the formation of C(sp^2)–B bonds. For instance, Ir-catalyzed intermolecular oxidative CH/BH cross-coupling of carboranyl

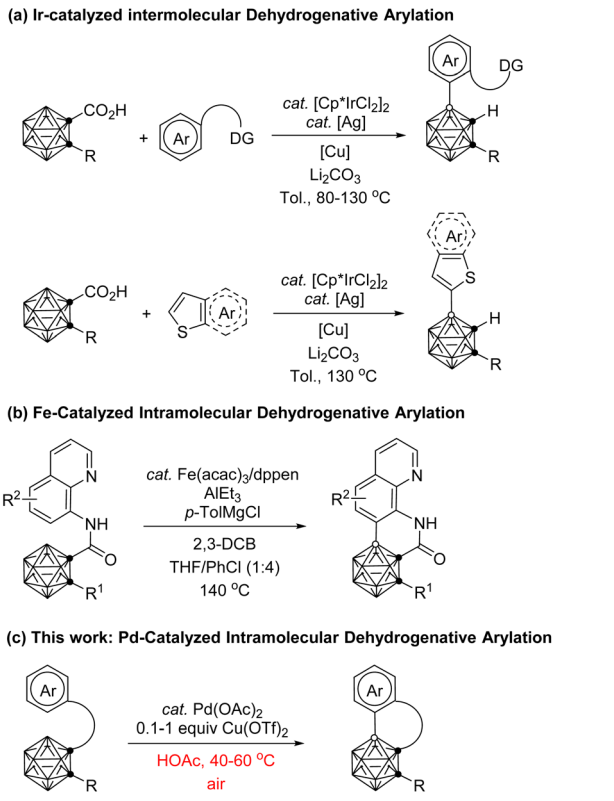

Scheme 1 Transition metal-catalyzed dehydrogenative arylation.

[a]*State Key Laboratory of Antiviral Drugs, Pingyuan Laboratory, School of Chemistry, and Chemical Engineering, Henan Normal University, Xinxiang, Henan 453007, China*
[b]*Shanghai-Hong Kong Joint Laboratory in Chemical Synthesis, Shanghai Institute of Organic Chemistry, University of Chinese Academy of Sciences, Chinese Academy of Sciences, Shanghai 200032, China. E-mail: zxie@cuhk.edu.hk; qiuzz@sioc.ac.cn*
[c]*Innovation Institute of Carbon Neutrality, International Joint Laboratory of Catalytic Chemistry, Department of Chemistry, College of Sciences, Institution, Shanghai University, Shanghai 200444, China*
[d]*Department of Chemistry, The Chinese University of Hong Kong, Shatin, N.T., Hong Kong, China*
[e]*Shenzhen Grubbs Institute, Department of Chemistry, Southern University of Science and Technology, Shenzhen 518055, China*

† Electronic supplementary information (ESI) available: Detailed experimental procedures for synthesis of compounds, NMR spectra and X-ray data. CCDC 2406471–2406482. For ESI and crystallographic data in CIF or other electronic format see DOI: https://doi.org/10.1039/d4sc08496a

carboxylic acid has been demonstrated with thiophene[7] and aryl substrates bearing various directing groups including carboxy,[8] amide,[9] and nitrogen-containing heterocycles (Scheme 1a).[10] Additionally, Fe-catalyzed intramolecular CH/BH oxidative cyclization of *o*-carborane with 8-aminoquinoline-based auxiliaries leads to the formation of C,B-substituted carborane-fused phenanthroline derivatives (Scheme 1b).[11]

These reactions generally require high temperatures and anhydrous/anaerobic reaction conditions for successful B–H activation. As part of an ongoing project in our laboratory, we aim to develop efficient and environmentally friendly methods for cage functionalization to synthesize boron-arylated *o*-carboranes with potential optoelectronic applications. We report here a Pd-catalyzed intramolecular aerobic oxidative dehydrocoupling of BH/CH between *o*-carborane and arenes with the construction of a series of five-, six- and seven-membered rings under mild reaction conditions (Scheme 1c).

Results and discussion

Our investigation began by examining the BH/CH oxidative coupling of 1-(2-methoxy-1-naphthyl)-2-benzyl-*o*-carborane (**1aa**) in the presence of $Pd(OAc)_2$ catalyst (10 mol%), H_2O_2 (1.0 equiv.) and TFA (1.0 equiv.) in HOAc at 40 °C in open air, giving acenaphtheno-*o*-carborane (**2aa**) with the construction of a boron-containing five-membered ring in 70% NMR yield (Table 1, entry 1). Screening of copper oxidants proved that $Cu(OTf)_2$ was the optimal choice, generating **2aa** in 96% yield (Table 1, entries 2–4). Compared with $Pd(OAc)_2$, $Pd(TFA)_2$ and $Pd(acac)_2$ gave slightly lower yield of **2aa**, whereas $Pd(MeCN)_4(BF_4)_2$ and $PdCl_2$ showed poor or no catalytic activity (Table 1, entries 5–8). Solvent was also very crucial for this

Table 1 Optimization of the conditions for 5-membered ring construction[a]

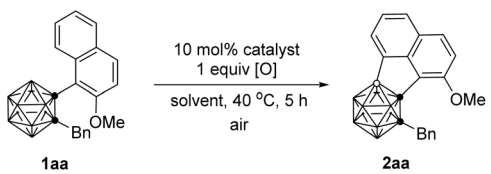

Entry	Catalyst	[O]	Solvent	Yield[b] (%)
1	$Pd(OAc)_2$	H_2O_2[c]	HOAc	70
2	$Pd(OAc)_2$	$Cu(OAc)_2$	HOAc	8
3	$Pd(OAc)_2$	$Cu(OPiv)_2$	HOAc	7
4	$Pd(OAc)_2$	$Cu(OTf)_2$	HOAc	96
5	$Pd(TFA)_2$	$Cu(OTf)_2$	HOAc	90
6	$Pd(acac)_2$	$Cu(OTf)_2$	HOAc	88
7	$Pd(MeCN)_4(BF_4)_2$	$Cu(OTf)_2$	HOAc	8
8	$PdCl_2$	$Cu(OTf)_2$	HOAc	N.R.
9	$Pd(OAc)_2$	$Cu(OTf)_2$	Toluene	16
10	$Pd(OAc)_2$	$Cu(OTf)_2$	THF	17
11	$Pd(OAc)_2$	$Cu(OTf)_2$	HFIP	30
12	$Pd(OAc)_2$	$Cu(OTf)_2$	TFA	78
13	$Pd(TFA)_2$	$Cu(OTf)_2$	TFA	90
14[d]	$Pd(OAc)_2$	$Cu(OTf)_2$	HOAc	78
15[e]	$Pd(OAc)_2$	$Cu(OTf)_2$	HOAc	72
16[f]	$Pd(OAc)_2$	$Cu(OTf)_2$	HOAc	44

[a] All reactions were carried out on 0.1 mmol scale in 1 mL of solvent. [b] NMR yield using 1,1,2,2-tetrachloroethane as an internal standard. [c] 1 equiv. of TFA was added. [d] 5 mol% $Pd(OAc)_2$. [e] 0.5 equiv. $Cu(OTf)_2$. [f] 25 °C, 12 h.

Table 2 Substrate scope of 5-membered ring construction[a,b]

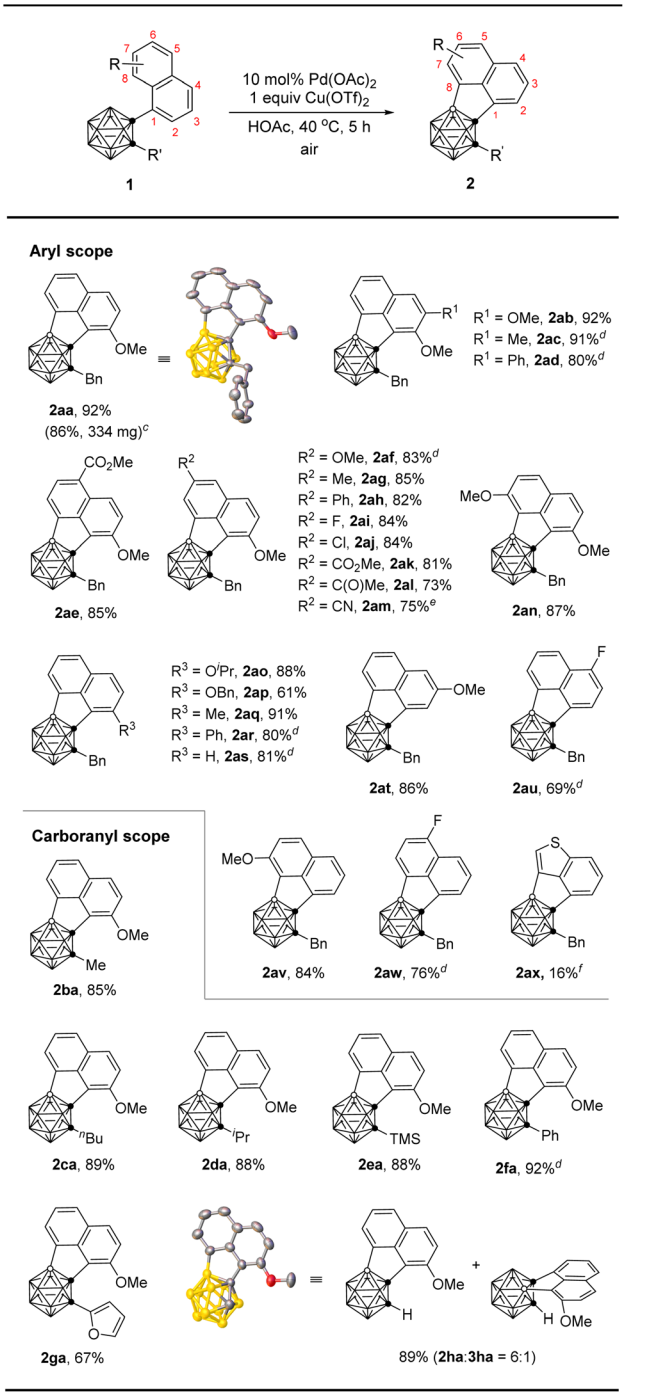

[a] All reactions were carried out on 0.2 mmol scale in 2 mL of HOAc. [b] Isolated yields. [c] The reaction was carried out on 1.0 mmol scale in 10 mL of HOAc. [d] 12 h. [e] 60 °C. [f] 80 °C, 24 h.

reaction. The use of toluene, THF, and 1,1,1,3,3,3-hexafluoro-2-propanol (HFIP) as the solvent gave the cross-coupling product in 16–30% yields. Trifluoroacetic acid (TFA) offered a reduced yield of 78% (Table 1, entries 9–12). While the use of $Pd(TFA)_2$ as catalyst and TFA as solvent led to a 90% yield of **2aa** (Table 1, entry 13). Further screening indicated that lowering the catalyst loading or oxidant amount resulted in reduced yields of **2aa** (Table 1, entries 14 and 15). Lowering reaction temperature to 25 °C led to poor reaction efficiency (Table 1, entry 16). In view of the yield of **2aa**, entry 4 was chosen as the optimal reaction conditions.

Under such optimized reaction conditions, the scope of this reaction was investigated and the results were compiled in Table 2. We first investigated the substrate generality of 2-methoxy-1-naphthyl group, affording the BH/CH dehydrocoupling products **2aa–2an** in 73–92% isolated yields. The mild reaction conditions were tolerant of a variety of functional groups including F, Cl, CO_2Me, C(O)Me and CN, and no obvious electronic effect was observed in **2aa–2an**. Notably, the reaction of substrate **1aa** proceeded smoothly on 1.0 mmol scale with a slightly lower efficiency (86% yield, 334 mg). Moreover, steric hindrance of 2-substitutions on naphthyl group did not affect the reaction efficiency (**2ao–2as**). 1-(1-Naphthyl)-2-benzyl-*o*-carborane **1as** also worked well, giving acenaphtheno-*o*-carborane product **2as** in 81% isolated yield, while variation of the R^3 group at 2-position of naphthyl had little effect on the reactivity for the formation of products **2ao–2ar**. 1-(1-Naphthyl)-2-benzyl-*o*-carboranes (**1a**) bearing –OMe or –F substituents at different position of the naphthyl group offered the corresponding products (**2at–2aw**) in 69–86% isolated yields. For **2at–2aw**, electron-donating units on naphthyl group generally offered better yields of **2a** than those of electron-withdrawing substituents. However, heteroaryl containing substrate **1ax** showed poor reactivity towards the BH/CH oxidative coupling between *o*-carborane and thienyl groups to afford **2ax** in only 16% isolated yield due probably to the interactions between Pd and S atoms. On the other hand, different substituents at cage C(2) were also evaluated, leading to the corresponding products **2ba–2ga** in moderate to excellent isolated yields. The results indicated that steric factor has an influence on the regioselectivity, as both B(4)- and B(3)-coupling products (**2ha** and **3ha**) were obtained with a molar ratio of 6 : 1 in the reaction of C(2)–H substrate **1ha**.

Furthermore, 1,2-di(1-naphthyl)-*o*-carborane (**4**) was also compatible with this five-membered ring construction process to afford B(4,7)- and B(4,11)-cross-coupling products **5** and **6** in 11% and 45% yields, respectively. The molecular structures of **2aa**, **2ha**, **5** and **6** were further confirmed by single-crystal X-ray analyses, supporting the unambiguous assignment of the substituted vertices (Scheme 2).

We then examined the feasibility of six-membered ring construction *via* BH/CH oxidative coupling using 1-(2-biphenyl)-2-benzy-*o*-carborane (**7a**) as a model substrate. Treatment of **7a** with 1 equiv. of $Cu(OTf)_2$ in the presence of 10 mol% of $Pd(OAc)_2$ catalyst in HOAc at 40 °C for 12 h afforded the desired product **8a** in 88% yield (Table 3, entry 1, standard conditions). Screening of other solvents and oxidants did not give better

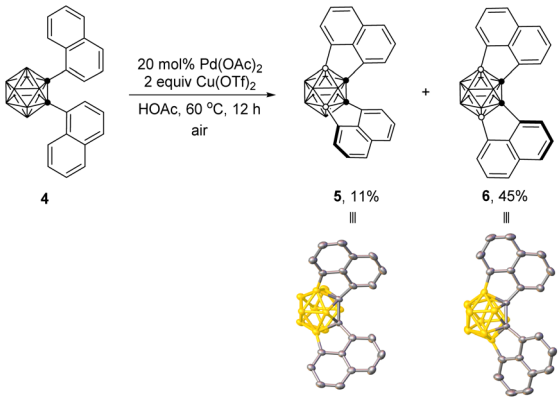

Scheme 2 Intramolecular dehydrogenative coupling of 1,2-dinaphthyl-*o*-carborane.

Table 3 Optimization of conditions for 6-membered ring construction[a]

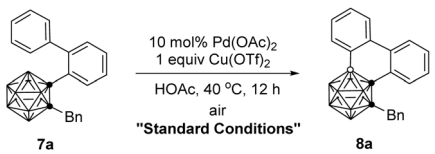

Entry	Variations from the "standard conditions"	Yield[b] (%)
1	None	88
2	HFIP instead of HOAc	26
3	THF instead of HOAc	13
4	$Cu(OAc)_2$ instead of $Cu(OTf)_2$	12
5	$Cu(OPiv)_2$ instead of $Cu(OTf)_2$	9
6	2 equiv. AgOTf instead of $Cu(OTf)_2$	20
7	1 equiv. H_2O_2/TFA instead of $Cu(OTf)_2$	8
8	5 mol% $Pd(OAc)_2$	59
9	0.5 equiv. $Cu(OTf)_2$	91
10	0.1 equiv. $Cu(OTf)_2$	75
11	0.1 equiv. $Cu(OTf)_2$, 60 °C, 5 h	90

[a] All reactions were carried out on 0.1 mmol scale in 1 mL of HOAc. [b] NMR yield using 1,1,2,2-tetrachloroethane as the internal standard.

results (Table 3, entries 2–7). Decreasing the catalyst loading to 5 mol% resulted in a decreased yield of **8a** (Table 3, entry 8). It is worth noting that lowering the amount of copper salt to 0.5 equiv. gave the product in 91% yield. Finally, using 0.1 equiv. of $Cu(OTf)_2$ as the cocatalyst and air as the oxidant led to 90% yield of **8a** at 60 °C (Table 3, entries 9–11).

With the optimized conditions in hand, we investigated the scope and limitation of this 6-membered ring construction (Table 4). The results indicated that both electron-donating and -withdrawing substituents at 4′- and 6′-positions of biphenyl group were well tolerated, leading to the desired products (**8a–8l**) in moderate to very good isolated yields (68–85%). In addition, the mild reaction conditions were tolerant of various functional groups, including halogens (**8e**, **8f**, **8k**, **8l**) and ester (**8g**). For C_{cage}-connected aromatic ring, biphenyls with substituents at 6- and 4-positions (**8m**, **8n** and **8q–8t**) gave very

Table 4 Substrate scope of 6-membered ring construction[a,b]

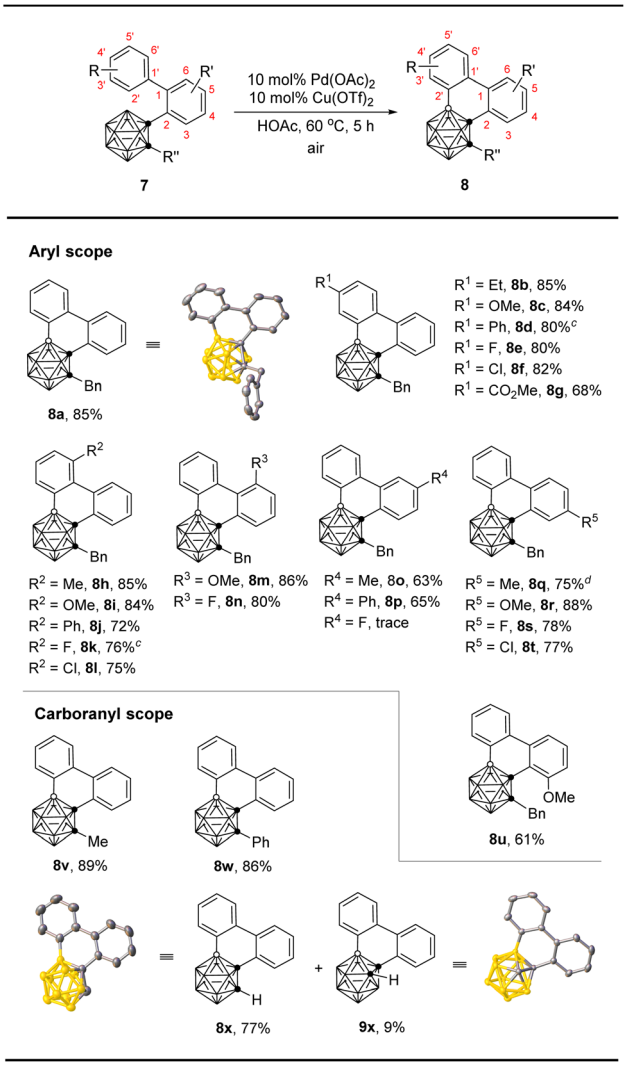

[a] All reactions were carried out on 0.2 mmol scale in 2 mL of HOAc. [b] Isolated yield. [c] 12 h. [d] 20 mol% $Cu(OTf)_2$, 12 h.

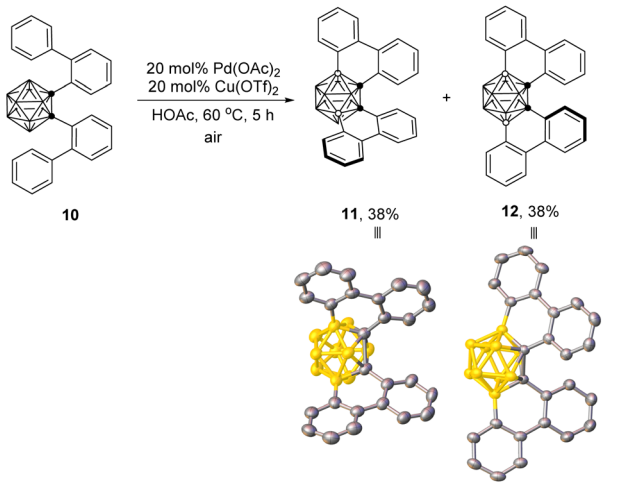

Scheme 3 Intramolecular dehydrogenative coupling of 1,2-dibiphenyl-*o*-carborane.

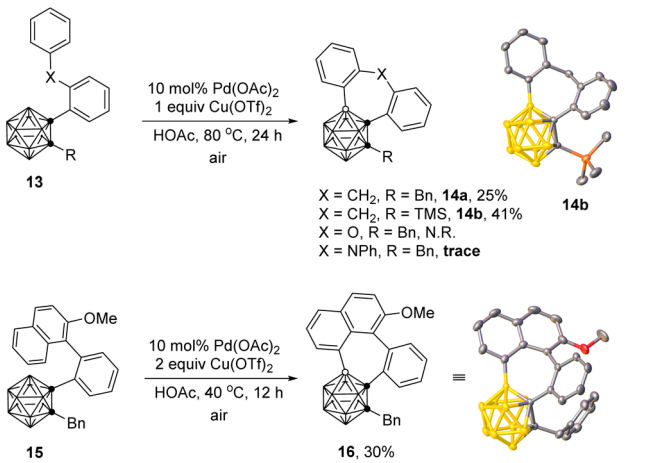

Scheme 4 Intramolecular dehydrogenative 7-membered ring construction.

high coupling efficiency (75–88%). However, those with 5-Me, 5-Ph, or 3-OMe substituents delivered the corresponding products (**8o**, **8p** and **8u**) in relatively lower yields (61–65%), while the use of 5-F substituent led to no reaction. Excellent yields were observed for C(2)-Me and -Ph substituted *o*-carboranophenanthrene products (**8v** and **8w**). With C(2)-H substrate **7x**, both 1,4- and 1,3-*o*-carborane fused phenanthrenes (**8x** and **9x**) were isolated in 77% and 9% yields, respectively, probably for steric reasons.

12-Dibiphenyl-*o*-carborane (**10**) also worked to afford the desired B(4,7)- and B(4,11)-crosscoupling products **11** and **12**, respectively, in the same 38% isolated yields in the presence of 20 mol% $Pd(OAc)_2$ and 20 mol% $Cu(OTf)_2$ in HOAc at 60 °C (Scheme 3). The B(4)-, B(3)-, B(4,7)- and B(4,11)-regioselectivities in **8a**, **8x**, **9x**, **11** and **12** were further confirmed by single-crystal X-ray analyses.

This strategy worked also for the synthesis of *o*-carborane fused seven-membered rings (Scheme 4). In the presence of 10 mol% $Pd(OAc)_2$ and 1 equiv. of $Cu(OTf)_2$, the intramolecular BH/CH oxidative coupling of 1-(2-(benzyl)phenyl)-*o*-carboranes **13** afforded the corresponding coupling products **14a** and **14b** in 25% and 41% yields, respectively. Instead of the methylene unit, substrates with X = O- or NPh-bridging moiety between the two phenyl groups showed poor reactivities for the seven-membered ring formation. In addition, such oxidative cross-coupling was compatible with 1-(2-(1-naphthyl)phenyl)-*o*-carborane substrate **15** with the employment of 2 equiv. of $Cu(OTf)_2$ to give **16** in 30% yield. Low yields may be related to unfavorable entropy and enthalpy strains in the formation of 7-membered rings.

To gain some insight into the reaction mechanism, several control experiments were carried out. The oxidative coupling reactions did not occur in the absence of palladium catalyst (Scheme 5a). The yield of **2aa** was dramatically dropped to 7%

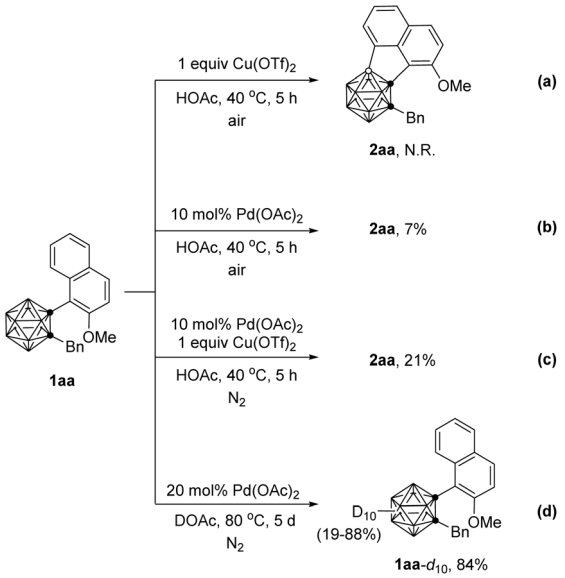

Scheme 5 Control experiments. (a) Reaction without $Pd(OAc)_2$. (b) Reaction without $Cu(OTf)_2$. (c) Reaction under N_2 atmosphere. (d) Palladium catalyzed BH deuteration in DOAc.

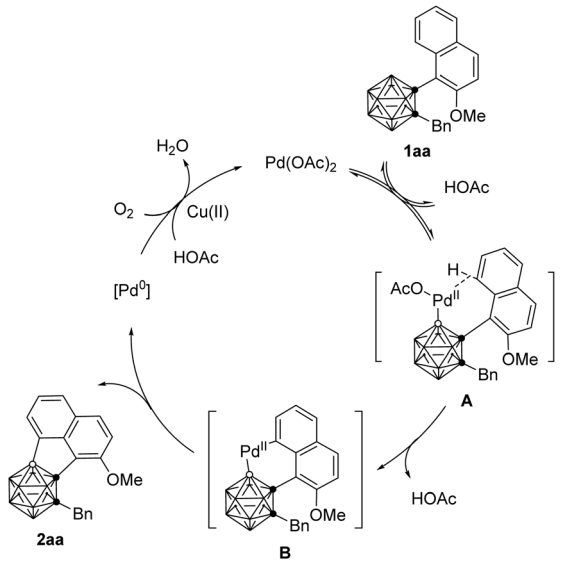

Scheme 6 Proposed reaction mechanism.

without $Cu(OTf)_2$ (Scheme 5b). In contrast, replacement of air with N_2 in the reaction system offered only a 21% yield of **2aa** under standard reaction conditions (Scheme 5c), suggesting that oxygen may act as an oxidant with the help of a Cu(II) cocatalyst.[12] To gain additional information regarding the initial step of the reaction, treatment of **1aa** with 20 mol% $Pd(OAc)_2$ under non-oxidative conditions using DOAc as the solvent led to 19–88% deuteration efficiency on the ten boron vertexes (Scheme 5d). These results indicated that B–H activation is more favorable than the aryl C–H activation in this Pd-catalyzed process, which is calculated [at the B3LYP level of theory in conjunction with the Lanl2dz basis set and the corresponding Hay–Wadt effective core potential (ECP) for Pd and standard 6-31+G** basis set for all remaining atoms] to be thermodynamically favorable with $\Delta G = -9.9$ kcal mol^{-1} (Fig. 1).

On the basis of the aforementioned experimental results and literature work,[13] a plausible reaction mechanism is proposed in Scheme 6. Electrophilic attack of the Pd(II) center at the B(4)–H affords an intermediate **A**, which undergoes intramolecular C–H bond activation to give the six-membered palladacycle **B**. It is noted that this reversible B–Pd bond formation will take place at all the ten BH vertexes of *o*-carborane cage, which follow the order B(3,6)–H ≪ B(4,5,7,11)–H < B(8,10)–H < B(9,12)–H relied on the differences in vertex charge.[14] Among these, only the B(3) and B(4)–Pd can approach the aromatic C–H due to the substrate configuration. The excellent B(4)-regioselectivity can be attributed to the electronic effect of the boron cage as well as the steric effect of C(2)-substituents. Reductive elimination affords the final products **2aa** with the release of Pd(0), followed by Cu(II) promoted the aerobic oxidation of Pd(0) to Pd(II).[12]

To further demonstrate the synthetic utility of the above intramolecular BH arylation protocol, 1-pyrenyl-*o*-carborane **17** was subjected to the palladium-catalyzed aerobic oxidative cross-coupling to afford the corresponding pyrene incorporated 1,4-disubstituted *o*-carborane **18** in 89% yield (Scheme 7). A single-crystal X-ray structure of **18** is shown in Fig. 2. The dihedral angle between the C_{cage}–C_{cage} bond and the pyrene moiety is about 43°. In the crystal packing diagram, there is no intermolecular π···π interaction due to the bulkiness of *o*-carboranyl unit, resulting in the suppressed ACQ effect. Moreover, one-dimensional continuous $B_{cage}H\cdots\pi$ interactions followed by the linear packing structure is observed.[15]

The photophysical properties of **18** were subsequently investigated. The UV/vis absorption spectrum of **18** in solution

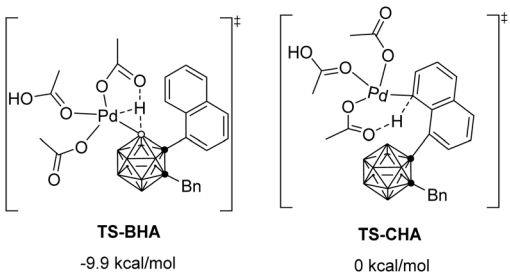

Fig. 1 Transition states calculated at the B3LYP/6-31+G**/Lanl2dz level of theory.

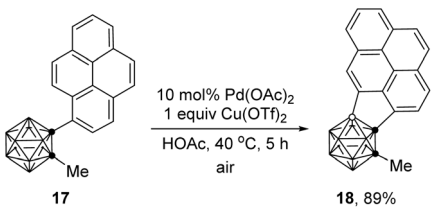

Scheme 7 Synthesis of carborane-fused polycyclic aromatic compound.

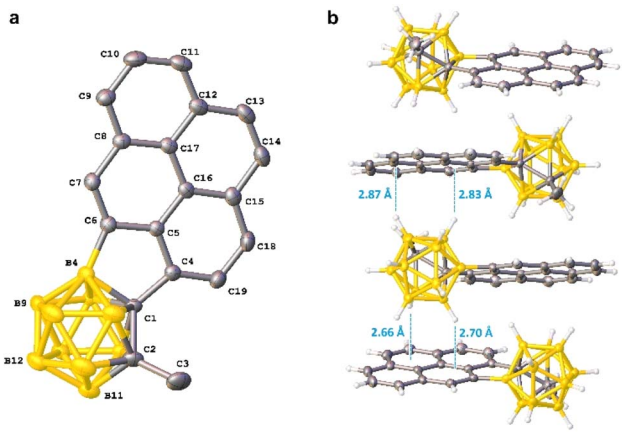

Fig. 2 (a) Molecular structure of **18**. Hydrogen atoms are omitted for clarity. (b) Packing structures of **18**.

was recorded and compared to those of pyrene and substrate **17**.[16] As shown in Fig. 3a, the absorption spectra of **17** and **18** exhibited bathochromic shifts relative to pyrene, which can be attributed to the involvement of the *o*-carborane unit in an extended π-conjugation.[17] On the other hand, the dual-emission bands were observed in the emission spectra of both **17** and **18**. While both **17** and **18** displayed emission peaks near 400 nm, their photoluminescence (PL) spectra differed significantly from pyrene, showing broad emission bands with peaks in the range of 570 to 600 nm (Fig. 3b). Furthermore, the B–C bond coupling in **17** caused a red-shifted emission, which was due to the increased electron-withdrawing effect of the

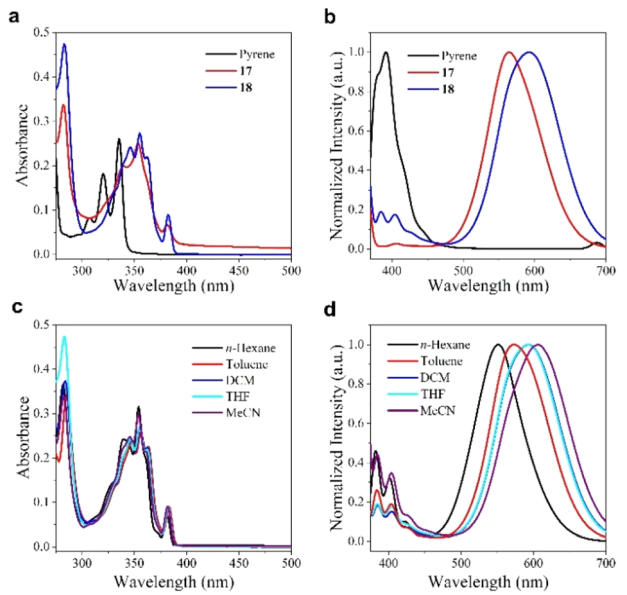

Fig. 3 (a) UV-vis absorption spectra of pyrene, **17** and **18** in THF ($c = 1.0 \times 10^{-5}$ M). (b) The normalized PL spectra of pyrene, **17** and **18** in THF ($c = 1.0 \times 10^{-5}$ M), the excitation wavelength is 340, 360 and 360 nm, respectively. (c) UV-vis absorption spectra of **18** in different solvents ($c = 1.0 \times 10^{-5}$ M). (d) The normalized PL spectra of **18** in different solvents ($c = 1.0 \times 10^{-5}$ M, $\lambda_{ex} = 360$ nm).

bisubstituted *o*-carborane.[18] To explore the dual-emission mechanism in **18**, changes in the absorption and PL spectra were monitored in solvents with varying polarities (Fig. 3c and d). No major peak shifts were observed in the absorption spectra, which could be attributed to the minimal solvent effect in the ground state. In contrast, as the solvent polarity increased, substantial bathochromic shifts were observed in the broad emission band at longer wavelengths in the PL spectra, suggesting that the luminescence near 600 nm in **18** is originated from the intramolecular charge transfer (ICT) state.[16,18] The fluorescence near 385 nm was largely unaffected by solvent polarity, displaying a mirror-image relationship with the absorption spectrum in the longer-wavelength region, thereby confirming its assignment to the locally excited (LE) state.[16]

Subsequently, the aggregation and solid-state emission properties of **18** were examined (Fig. 4 and Table 5). In a study involving THF/water mixtures, a THF solution of **18** emitted yellow light at 590 nm due to its ICT emission. As the water fraction (f_w) in the mixture increased from 0% to 60%, the emission intensity gradually decreased, and the spectrum exhibited a continuous red shift, which can be attributed to the ICT effect.[19] With further increases in f_w, the emission intensity significantly increased again, accompanied by a gradual blue shift. In the aqueous mixture with f_w of 99%, the emission shifted to 567 nm. Additionally, a higher quantum efficiency (94%) was observed for the powder sample compared to the THF solution and the aggregated state, indicating that **18**

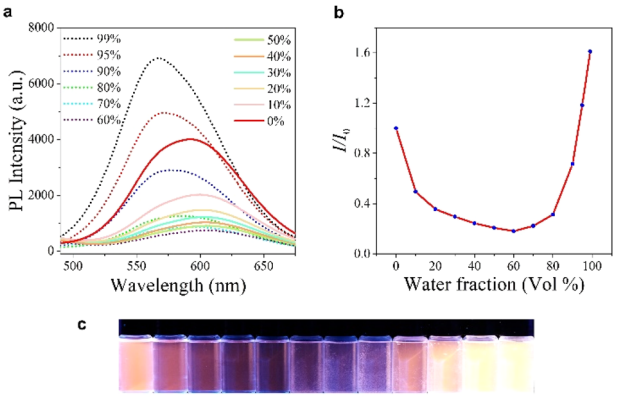

Fig. 4 (a) Emission spectra of **18** in the binary THF/H_2O solution with different volumetric ratios (f_w, vol%) of water ($c = 100$ μM, $\lambda_{ex} = 360$ nm). (b) Dependence of I/I_0 ratios of **18** in THF with different water fractions. (c) Photographs of **18** in THF/H_2O solution with various fractions of water (f_w) taken under UV light (365 nm).

Table 5 Summary of emission properties of **18**

	$\lambda_{em}{}^a$ (nm)	$\Phi_{PL}{}^b$ (%)	τ_F (ns)
THF	384, 404, 590	17.7	6.0
99% H_2O	567	34.5	9.8
Solid	570	94.1	7.9

[a] Excited at 360 nm. [b] Determined as an absolute value.

exhibits both aggregation-induced emission (AIE) and AIE enhancement (AIEE) properties. For this arylated *o*-carborane with a fused structure at the neighboring carbon and boron atoms for fixing molecular conformation, the elongation of the C_{cage}–C_{cage} bond in the excited state, followed by nonradiative decay, was proposed as the primary mechanism for emission quenching in solution.[20]

Conclusions

In summary, an efficient intramolecular aerobic Pd-catalyzed BH/CH oxidative coupling has been achieved, leading to the facile synthesis of previously unavailable carborane-fused five-, six- and seven-membered ring structures under mild conditions. A plausible reaction mechanism including sequential electrophilic B–H and C–H activation, and reductive elimination was proposed, which is supported by the deuterium labeling experiment and DFT calculations. The facile synthesis has potential application in carborane-based luminogens.

Data availability

The experimental procedures and additional data can be found in the ESI.† Crystallographic data for the structures reported in this article have been deposited at the Cambridge Crystallographic Data Centre, under deposition number 2406471 (**2aa**), 2406472 (**2ha**), 2406473 (**5**), 2406474 (**6**), 2406475 (**8a**), 2406476 (**8x**), 2406477 (**9x**), 2406478 (**11**), 2406479 (**12**), 2406480 (**14b**), 2406481 (**16**), and 2406482 (**18**). Copies of the data can be obtained free of charge from the CCDC *via* **https://www.ccdc.cam.ac.uk/structures/**.

Author contributions

Z. Q. and Z. X. directed and conceived this project. Z. W. and J. Y. conducted the experiments. J. Z. did the theoretical work. All authors discussed the results and wrote the manuscript.

Conflicts of interest

There are no conflicts to declare.

Acknowledgements

This work was supported by grants from the National Natural Science Foundation of China (Project No. 22371290 and 92056106 to Z. Q.; Project No. 22331005 to Z. X.), Shenzhen Science and Technology Program (Project No. KQTD20221101093558015 to Z. X.), and the Shanghai-Hong Kong Joint Laboratory in Chemical Synthesis, CAS.

Notes and references

1 (*a*) R. N. Grimes, *Carboranes*, Academic Press, Amsterdam, The Netherlands, 3rd edn, 2016; (*b*) N. S. Hosmane and R. D. Eagling, *Handbook of Boron Science*, World Scientific, 2018, vol. 2, pp. 1–155; (*c*) J. Poater, C. Viñas, M. Sola and F. Teixidor, *Nat. Commun.*, 2022, **13**, 3844; (*d*) F. Sun, S. Tan, H.-J. Cao, C.-S. Lu, D. Tu, J. Poater, M. Solà and H. Yan, *J. Am. Chem. Soc.*, 2023, **145**, 3577–3587.

2 (*a*) R. Núñez, M. Tarrés, A. Ferrer-Ugalde, F. F. de Biani and F. Teixidor, *Chem. Rev.*, 2016, **116**, 14307; (*b*) S. Mukherjee and P. Thilagar, *Chem. Commun.*, 2016, **52**, 1070–1093; (*c*) X. Li, H. Yan and Q. Zhao, *Chem.–Eur. J.*, 2016, **22**, 1888–1898; (*d*) R. Núñez, I. Romero, F. Teixidor and C. Viñas, *Chem. Soc. Rev.*, 2016, **45**, 5147–5173; (*e*) B. P. Dash, R. Satapathy, J. A. Maguire and N. S. Hosmane, *New J. Chem.*, 2011, **35**, 1955–1972.

3 (*a*) M. F. Hawthorne and A. Maderna, *Chem. Rev.*, 1999, **99**, 3421–3434; (*b*) M. Scholz and E. Hey-Hawkins, *Chem. Rev.*, 2011, **111**, 7035–7062; (*c*) P. Stockmann, M. Gozzi, R. Kuhnert, M. B. Sárosi and E. Hey-Hawkins, *Chem. Soc. Rev.*, 2019, **48**, 3497–3512; (*d*) K. Fink and M. Uchman, *Coord. Chem. Rev.*, 2021, **431**, 213684.

4 (*a*) K. Kokado and Y. Chujo, *J. Org. Chem.*, 2011, **76**, 316–319; (*b*) A. M. Spokoyny, C. W. Machan, D. J. Clingerman, M. S. Rosen, M. J. Wiester, R. D. Kennedy, C. L. Stern, A. A. Sarjeant and C. A. Mirkin, *Nat. Chem.*, 2011, **3**, 590–596.

5 (*a*) K. Kokado and Y. Chujo, *Macromolecules*, 2009, **42**, 1418–1420; (*b*) K. R. Wee, Y. J. Cho, J. K. Song and S. O. Kang, *Angew. Chem., Int. Ed.*, 2013, **52**, 9682–9685; (*c*) H. Naito, Y. Morisaki and Y. Chujo, *Angew. Chem., Int. Ed.*, 2015, **54**, 5084–5087; (*d*) D. Tu, P. Leong, S. Guo, H. Yan, C. Lu and Q. Zhao, *Angew. Chem., Int. Ed.*, 2017, **56**, 11370–11374; (*e*) X. Li, Y. Yin, H. Yan and C. Lu, *Chem.–Asian J.*, 2017, **12**, 2207–2210; (*f*) R. Huang, H. Liu, K. Liu, G. Wang, Q. Liu, Z. Wang, T. Liu, R. Miao, H. Peng and Y. Fang, *Anal. Chem.*, 2019, **91**, 14451–14457; (*g*) X. Wei, M. J. Zhu, Z. Cheng, M. Lee, H. Yan, C. Lu and J. J. Xu, *Angew. Chem., Int. Ed.*, 2019, **58**, 3162–3166; (*h*) J. Ochi, K. Tanaka and Y. Chujo, *Angew. Chem., Int. Ed.*, 2020, **59**, 9841–9855; (*i*) K. Tanaka, M. Gon, S. Ito, J. Ochi and Y. Chujo, *Coord. Chem. Rev.*, 2022, **472**, 1–34; (*j*) Z. Wang, X. Gou, Q. Shi, K. Liu, X. Chang, G. Wang, W. Xu, S. Lin, T. Liu and Y. Fang, *Angew. Chem., Int. Ed.*, 2022, **61**, e202207619; (*k*) H. Yang, H. Liu, Y. Shen, S. T. Zhang, Q. Zhang, Q. Song, C. Lv, C. Zhang, B. Yang, Y. Ma and Y. Zhang, *Angew. Chem., Int. Ed.*, 2022, **61**, e202115551; (*l*) R. Chen, J. Liu, C. Lin, Y. Li, Y. Geng and Y. Yuan, *Chin. Chem. Lett.*, 2024, **35**, 110074; (*m*) T. Lee, J. H. Jang, N. N. T. Nguyen, J. Jung, J. H. Lee and M. H. Lee, *Adv. Sci.*, 2024, **11**, 2309016; (*n*) K. Yuhara and K. Tanaka, *Angew. Chem., Int. Ed.*, 2024, **63**, e202319712; (*o*) Z. Sun, J. Zong, H. Ren, C. Lu, D. Tu, J. Poater, M. Solà, Z. Shi and H. Yan, *Nat. Commun.*, 2024, **15**, 7934.

6 (*a*) Y. Quan, Z. Qiu and Z. Xie, *Chem.–Eur. J.*, 2018, **24**, 2795–2805; (*b*) Y. Quan and Z. Xie, *Chem. Soc. Rev.*, 2019, **48**, 3660–3673; (*c*) Y. K. Au and Z. Xie, *Bull. Chem. Soc. Jpn.*, 2021, **94**, 879–899; (*d*) Z. Qiu and Z. Xie, *Acc. Chem. Res.*, 2021, **54**, 4065–4079.

7 Y. Quan, H. Lyu and Z. Xie, *Chem. Commun.*, 2017, **53**, 4818–4821.

8 Y. K. Au, H. Lyu, Y. Quan and Z. Xie, *Chin. J. Chem.*, 2020, **38**, 383–388.

9 (*a*) Y. K. Au, H. Lyu, Y. Quan and Z. Xie, *J. Am. Chem. Soc.*, 2019, **141**, 12855–12862; (*b*) K. Cao, J. Wu, C. Y. Zhang, L. F. Ding and J. Yang, *ChemistrySelect*, 2021, **6**, 10178–10181.
10 Y. Chen, Y. Quan and Z. Xie, *Chem. Commun.*, 2020, **56**, 7001–7004.
11 Y. Chen, H. Lyu, Y. Quan and Z. Xie, *Org. Lett.*, 2021, **23**, 4163–4167.
12 (*a*) J. P. Parrish, Y. C. Jung, S. I. Shin and K. W. Jung, *J. Org. Chem.*, 2002, **67**, 7127–7130; (*b*) B. J. Li, S. L. Tian, Z. Fang and Z. J. Shi, *Angew. Chem., Int. Ed.*, 2008, **47**, 1115–1118; (*c*) P. Kannaboina, K. A. Kumar and P. Das, *Org. Lett.*, 2016, **18**, 900–903; (*d*) D. Wang and S. S. Stahl, *J. Am. Chem. Soc.*, 2017, **139**, 5704–5707; (*e*) S. J. Tereniak, D. L. Bruns and S. S. Stahl, *J. Am. Chem. Soc.*, 2020, **142**, 20318–20323.
13 (*a*) C. S. Yeung and V. M. Dong, *Chem. Rev.*, 2011, **111**, 1215–1292; (*b*) C. Liu, J. Yuan, M. Gao, S. Tang, W. Li, R. Shi and A. Lei, *Chem. Rev.*, 2015, **115**, 12138–12204; (*c*) Y. Yang, J. Lan and J. You, *Chem. Rev.*, 2017, **117**, 8787–8863.
14 F. Teixidor, G. Barberà, A. Vaca, R. Kivekäs, R. Sillanpää, J. Oliva and C. Viñas, *J. Am. Chem. Soc.*, 2005, **127**, 10158–10159.
15 X. Zhang, H. Dai, H. Yan, W. Zou and D. Cremer, *J. Am. Chem. Soc.*, 2016, **138**, 4334–4337.
16 (*a*) K. Nishino, H. Yamamoto, K. Tanaka and Y. Chujo, *Org. Lett.*, 2016, **18**, 4064–4067; (*b*) X. Wu, J. Guo, J. Zhao, Y. Che, D. Jia and Y. Chen, *Dyes Pigm.*, 2018, **154**, 44–51; (*c*) S. Kim, J. H. Lee, H. So, M. Kim, M. S. Mun, H. Hwang, M. H. Park and K. M. Lee, *Inorg. Chem. Front.*, 2020, **7**, 2949–2959.
17 B. P. Dash, R. Satapathy, E. R. Gaillard, K. M. Norton, J. A. Maguire, N. Chug and N. S. Hosmane, *Inorg. Chem.*, 2011, **50**, 5485–5493.
18 (*a*) Y. Yin, X. Li, S. Yan, H. Yan and C. Lu, *Chem.–Asian J.*, 2018, **13**, 3155–3159; (*b*) L. Guo, X. Yu, J. Du, W. Li, V. Bregadze, D. Tu, C. Lu and H. Yan, *Chem.–Eur. J.*, 2022, **28**, e202200303; (*c*) M. Zhu, Q. Zhou, H. Cheng, Z. Meng, L. Xiang, Y. Sha, H. Yan and X. Li, *New J. Chem.*, 2022, **46**, 11382–11388; (*d*) W. Fang, K. Liu, G. Wang, Y. Liang, R. Huang, T. Liu, L. Ding, J. Peng, H. Peng and Y. Fang, *Anal. Chem.*, 2021, **93**, 8501–8507; (*e*) J. Tong, Y. Cao, Y. W. Zhang, P. Wang, P. Wang, X. J. Liao, W. Zhang, Y. Wang, Y. X. Zheng, J. J. Zhu and Y. Pan, *Angew. Chem., Int. Ed.*, 2022, **61**, e202209438.
19 (*a*) R. Hu, E. Lager, A. Aguilar-Aguilar, J. Liu, J. W. Y. Lam, H. H. Y. Sung, I. D. Williams, Y. Zhong, K. S. Wong, E. Peña-Cabrera and B. Z. Tang, *J. Phys. Chem. C*, 2009, **113**, 15845–15853; (*b*) E. Wang, J. W. Y. Lam, R. Hu, C. Zhang, Y. S. Zhao and B. Z. Tang, *J. Mater. Chem. C*, 2014, **2**, 1801–1807.
20 (*a*) J. Ochi, K. Tanaka and Y. Chujo, *Dalton Trans.*, 2021, **50**, 1025–1033; (*b*) J. Ochi, T. Yanagihara, K. Tanaka and Y. Chujo, *Phys. Chem. Chem. Phys.*, 2023, **25**, 11839–11844.